Supplemental Materials

Pathway Verification in TX-TL

Linear DNA encoding individual enzymes are added into TX-TL reactions to verify enzyme expression. End products of TX-TL reactions are directly used for polyacrylamide gel electrophoresis with sodium dodecyl sulfate (SDS-PAGE) preparation, and all enzymes of the BDO pathway show up on the gel at expected sizes. Below **Figure S1** shows an SDS-PAGE gel with the expression of relevant pathway enzymes. 0.5 ul of TX-TL reactions are used for analyzing enzyme expression. Background proteins are proteins extracted during cell lysis.

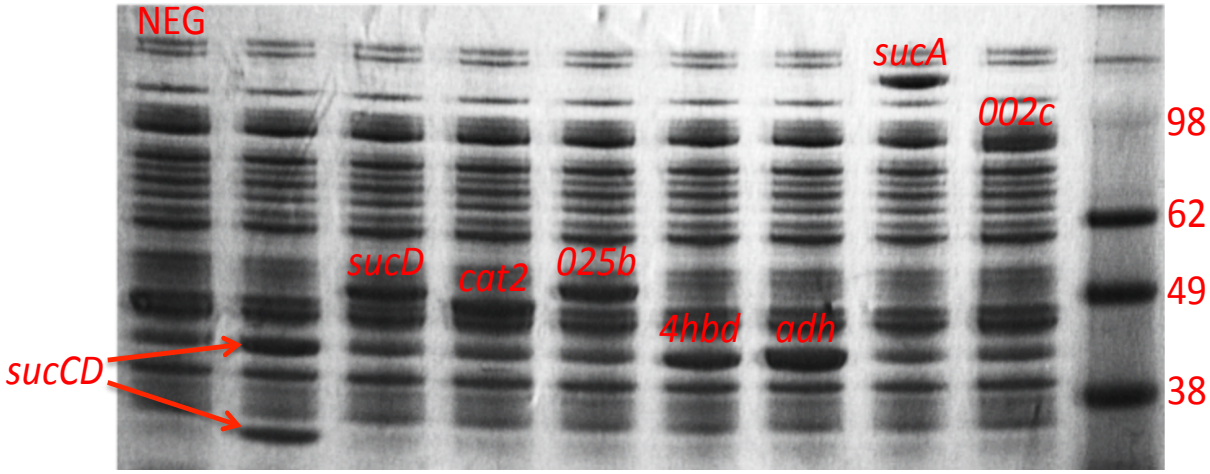

Figure S1: Verifying enzyme expression using SDS-PAGE gel: From left to right are negative control (NEG), succinyl-CoA synthetase (*sucCD*, two subunits α and β at 29.6 kDa and 41.4 kDa[1]), CoA-dependent succinate semialdehyde dehydrogenase (*sucD-035*, 50.2 kDa), 4-hydroxybutyryl-CoA transferase (*cat2-034*, 48.0 kDa), 4-hydroxybutyryl-CoA reductase (*ald-025B*, 52.1 kDa), 4-hydroxybutyrate dehydrogenase (*4hbd-036*, 41.3 kDa) alcohol dehydrogenase (*adh-012*, 43.1 kDa), 2-oxoglutarate decarboxylase (*sucA*, 100kDa), 4-hydroxybutyryl-CoA reductase (*ald(002c)*, 95.3kDa), and protein ladder.

A range of cofactor concentration were tested for improved BDO production. Results are shown in **Figure S2**. In a typical TX-TL reaction, 0.26 mM of coA has been added as part of the buffer, 1 mM of NADPH, 1 mM of acetyl-coA, and 1 mM of NADH are added. Here, we vary the concentration of coA, acetyl-coA, NADP, and NADPH one at a time to understand the effect of these cofactors have on the metabolite production. The metric here is to compare downstream metabolite production versus upstream metabolite production. Mainly, we are comparing the total production of BDO and GBL to the total production of GABA and 4HB. **Figure S2** shows that the lack of coA or acetyl-coA leads to the accumulation of upstream metabolites. When more NADPH is added to the system, more downstream metabolites are produced.

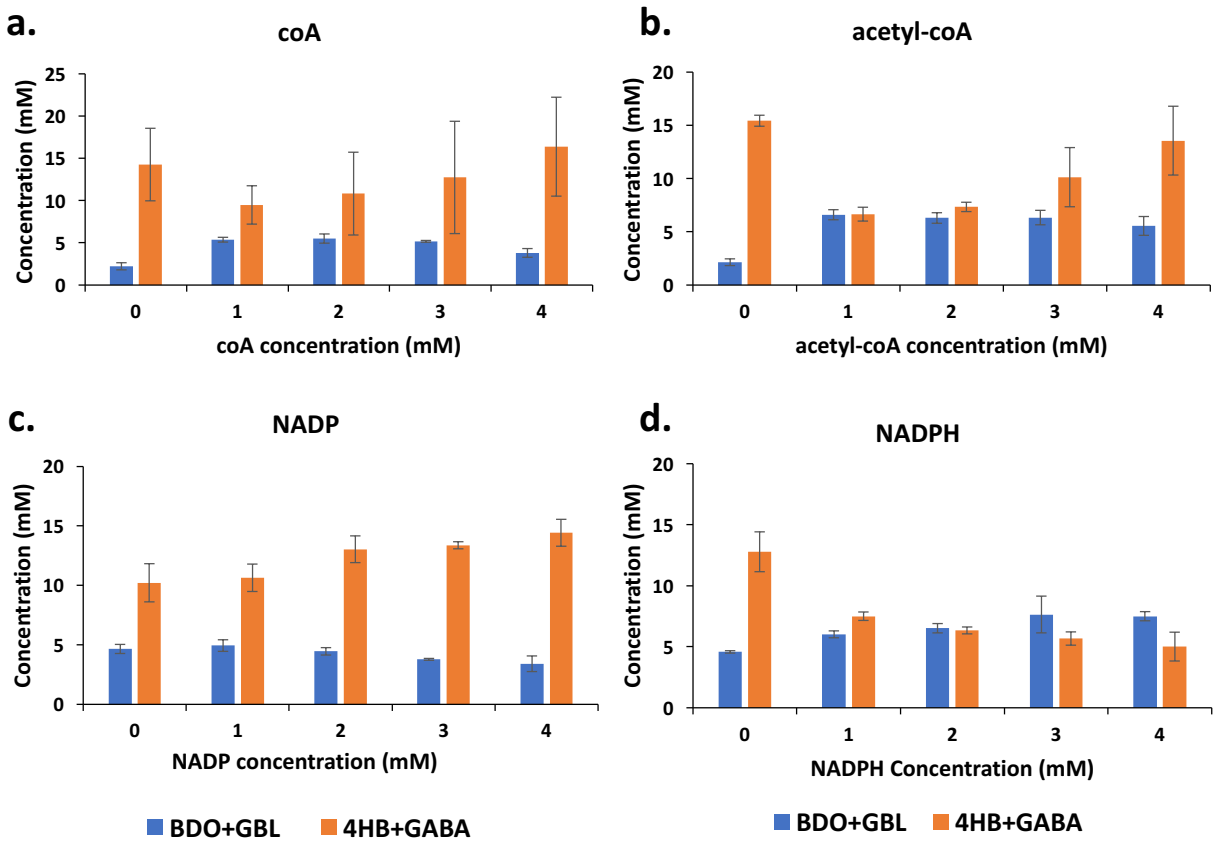

Figure S2: Testing cofactor concentration for improved BDO production: a. coA b. acetyl-coA c. NADP d. NADPH, blue bar—sum of the concentration of BDO and GBL, orange bar—sum of the concentration of 4HB and γ-aminobutyric acid (GABA). Error bars show one standard deviation for n ≥ 3 independent experiments.

System-level Studies of TX-TL

The production of acetate is very prominent in the TX-TL system. The production of acetate through the BDO pathway enzymes does not account for the acetate measured in the system. The conversion from 3-PGA or glutamate to acetate regenerates cofactor such as NADH, NADPH, ATP, and acetyl-coA, which explains the significant production of acetate.[2] **Figure S3b and Figure S3c** below shows the ratio of NADPH/NADP and NADH/NAD. The energy charge is also calculated to capture resource limitation of the system (shown in **Figure S3a**). The production of HB-coA in **Figure S3d** shows the peak at 6 hours, which is when BDO production starts to plateau.

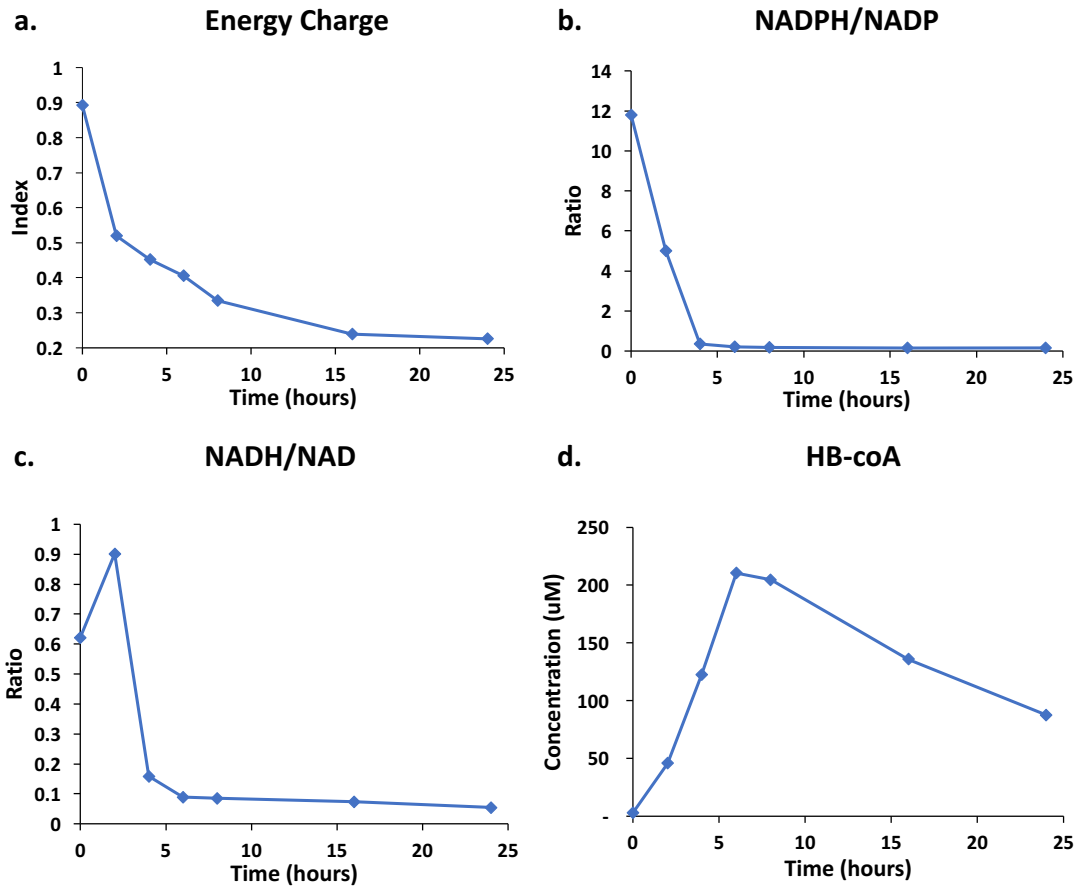

Figure S3: Metabolomics in TX-TL: a. Energy Charge over time b. Ratio of NADPH/NADP c. Ratio of NADH/NAD d. HB-coA concentration over time

Genomatica has previously developed antibodies specifically for enzyme *ald* and *adh*. Without inserting additional protein tags, we analyze enzyme expression profile without interfering pathway dynamics. Below in **Figure S4** shows the SDS-PAGE (top) and Western blot (bottom) that analyzed the protein dynamics over time. The protein bands in the Western blot show unspecific binding at 30 kDa and 80 kDa. However, the separation between target protein band and the unspecific band are large enough for protein expression analysis. As shown, the *ald* (*C*) is about 60 kDa, where the *adh* (*C*) is about 40 kDa. We analyzed the same sample in two different ways: 1) add TX-TL reaction directly for protein gel analysis and 2) centrifuge samples and add soluble fraction for protein gel analysis. The protein analysis shows that TX-TL is a good expression system where there is a good amount of protein remains in the soluble fraction. Here we can also visually identify that protein expression peaks at 8 hours.

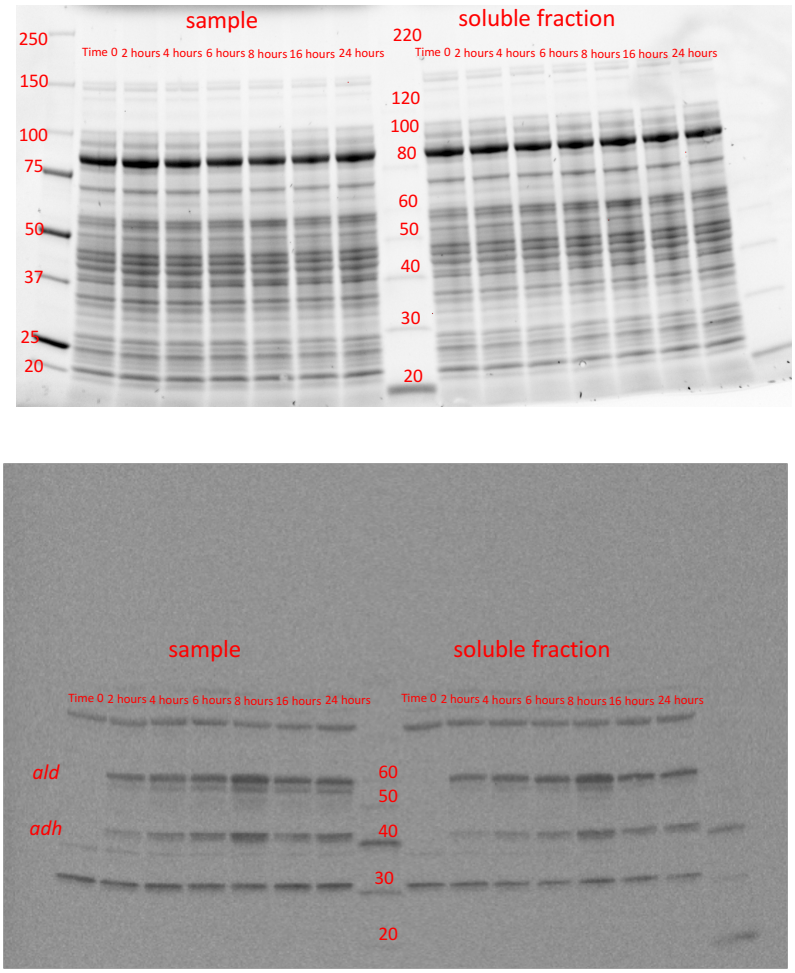

Figure S4: *ald* (*C*) and *adh* (*C*) expression over time in TX-TL. Top: SDS-PAGE gel. Bottom: Western blot. Both images are separated by total sample (left) and soluble protein fraction (right). *ald* (*C*) and *adh* (*C*) are 60kDa and 40 kDa respectively.

Design Space Exploration

We have picked elements from Chen *et al.*'s terminator library:[3] ECK120033736 (164.6x), ECK120015440 (119.21x), and ECK120010799 (101.05x). These terminators have been previously tested for similar expression levels. We use plasmids pZ33s and pZS*23s previously published.[4] Detailed constructs are shown in **Figure S5**. We use BCD22 for enzymes on the pZA33s plasmid. BCD 22 is the UTR that gives weak protein expression, and pZA33s has p15A as a replication of origin. pZS*23S has SC101 as a replication of origin. The pZA33s plasmid has a slightly higher copy number than the pZS*23S. For experiments done during design space exploration, 5 nM of the pZA33s is added, and 3 nM of pZS*23s is added. The ratio used in TX-TL is an attempt to reflect the copy number ratio *in vivo*. PZA33s contains kanamycin resistance, and pZS*23s contains chloramphenicol resistance. While kanamycin kills bacteria by binding to 30S ribosomal subunit and causes misreading of t-RNA, chloramphenicol kills bacteria by binding to 50S ribosomal subunit and prevents peptide bond formation.[5] To better map TX-TL to *in vivo*, it may also be a good idea to switch to a different set of antibiotics.

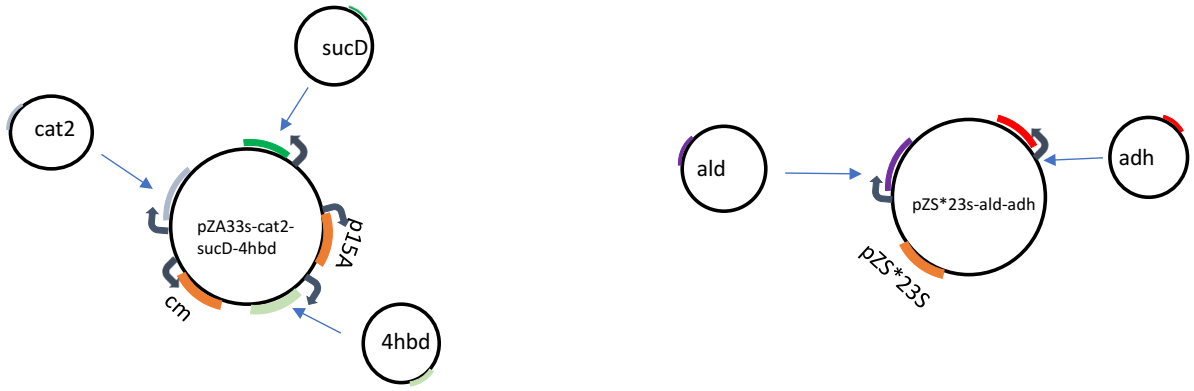

Figure S5: Construct assembly for design space exploration. Left: non-bottleneck enzymes *sucD*, *cat2*, and *4hbd* on pZA33s. Right: bottleneck enzymes *ald* and *adh* on pZS*23s

Constructs are designed to mimic the ratio of linear DNA encoding pathway enzymes. The metabolic profile of TX-TL reaction added with plasmid DNA is similar to the metabolic profile of TX-TL reaction added with linear DNA. **Table S1** shows the constructs with varying *ald* (*C*) and *adh* (*C*) strength. The numbers in the table are the order of which the samples are loaded onto the protein gel for expression comparison between TX-TL and *in vivo*.

Sample Order		*adh* Expression Level		
		Strong	Medium	Weak
ald Expression Level	Strong	1	2	3
	Medium	4	5	6
	Weak	7	8	9

Table S1: Constructs with varying *ald* (*C*) and *adh* (*C*) expression levels: The numbers in the table are the order in which samples are loaded onto protein gels for expression comparison shown in **Figure S7**.

Samples for metabolite analysis and protein expression analysis are collected after 16 hours of TX-TL reaction. The raw SDS-PAGE and Western blots are shown in **Figure S6**. Protein ladder followed by the negative control are added as the two samples. Constructs with varying *adh*(*C*) and *ald* (*C*) expression levels shown in **Table S1** then added by its numerical order. Values presented in **Figure 3** are intensities of soluble protein from the Western blot, which are measured and normalized by the total protein intensities shown in the SDS-PAGE gel. Overall, **Figure S6b** and **S6d** shows a range of protein expression levels for *adh* (*C*) and *ald* (*C*). Note that there are more unspecific bands in the Western blot for *in vivo* samples. We have observed insoluble proteins in the *in vivo* samples, which explains the smear on the right side of the Western blot shown in **Figure S6d**. **Table S2** lists the parameters from linear regression for data shown in **Figure 3 c** and **f**. The slope differences in TX-TL indicates that resource limitation might have played a role in metabolite production. The strong expression of *adh* (*C*) may have impacted metabolite production, where too weak of an expression is not enough for metabolite

production. The slope of the linear regression for *in vivo* data is very similar, which confirms that *ald* (*C*) is the bottleneck enzyme for the production of BDO.

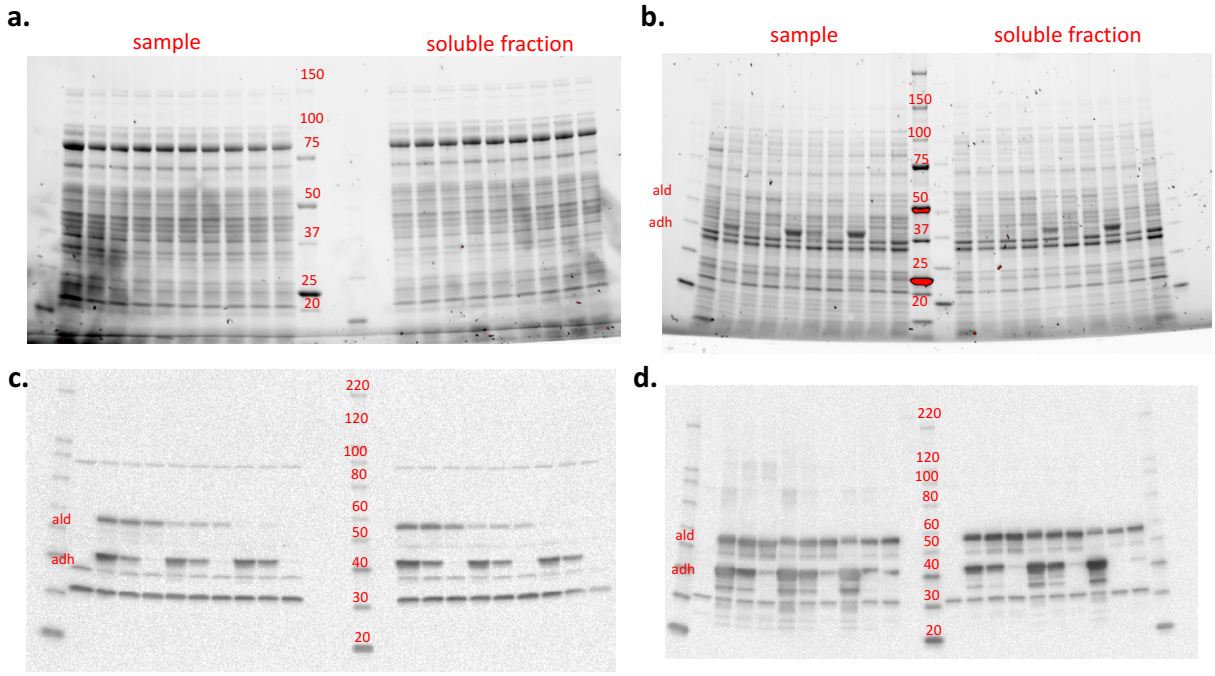

Figure S6: *ald* (*C*) and *adh* (*C*) expression *in vivo* (right: **b** and **d**) Vs. in TX-TL (left: **a** and **c**). Top: SDS-PAGE gel (**a** and **b**). Bottom: Western blot (**c** and **d**). Each image is separated by total sample (left) and soluble protein fraction (right). *ald* (*C*) and *adh* (*C*) are 60kDa and 40 kDa respectively.

Linear Regression Parameters in **Figure 3c**		
adh Expression	slope	intercept
Strong	5.32	2.09
Medium	9.52	1.90
Weak	5.52	1.50

Linear Regression Parameters in **Figure 3f**		
adh Expression	slope	intercept
Strong	0.24	0.94
Medium	4.49	-0.17
Weak	6.26	-1.18

Table S2: Slope and Intercept for Linear Regression in **Figure 3**.

Applications of TX-TL

Enzyme expressions from two of the three enzyme combinations are analyzed. Details are shown in **Figure S7**. Time-course protein expression (1 hour, 3hours, 5 hours, and 8 hours) of

Combination B and Combination C are analyzed. From left to right of the Western blot, a negative control was added first, and time-course samples from Combination B and Combination C were added. To the left of the Western blot is the relative *ald* expression over time. Note that enzymes from Combination C have a strong expression than enzymes from Combination B. Both *ald* and *adh* from Combination C are enzymes engineered for stability *in vitro*, while the ones from Combination B are wild-type enzymes.

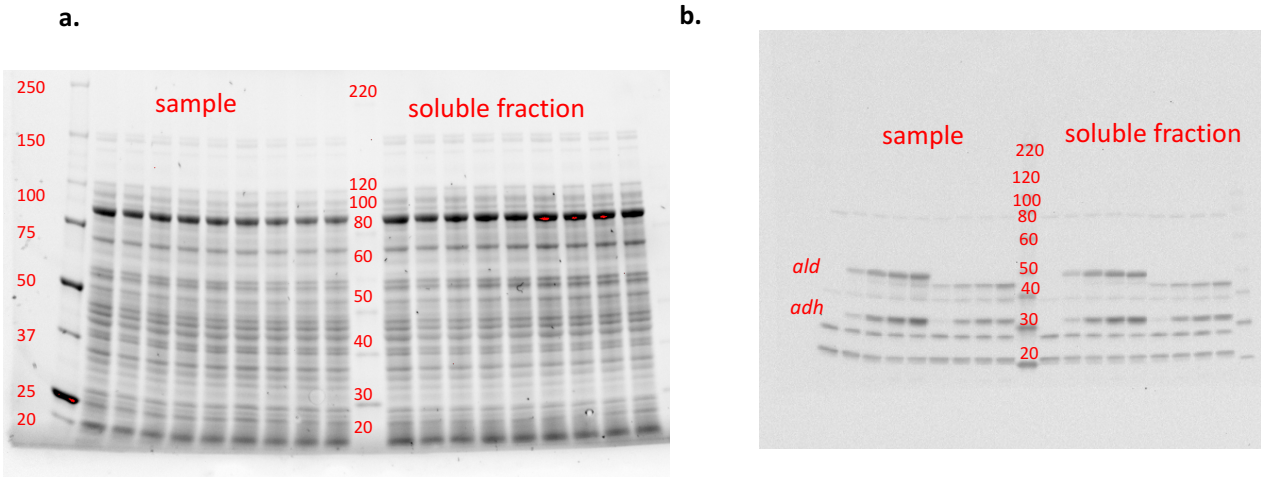

Figure S7: *ald* and *adh* expression for ranking pathways in TX-TL. To the left of the ladder are samples from total TX-TL reactions, and to the right of the ladder is soluble protein in the supernatant fraction of TX-TL reactions.

Characteristics of S138 *in vivo*

Metabolomics of S138 *in vivo* is also performed. Below in **Figure S8** shows the production of BDO over time. Energy charge (**Figure S8b**), NADPH/NADP ratio (**FigureS8c**), and NADH/NAD ratio (**Figure S8d**) are very similar to the ones observed in TX-TL. The pH *in vivo* drops rapidly (**Figure S9b**), and it is about 4 by the end of 28 hours, where the pH in TX-TL stays above 6 during 8-hour reactions. Improvement on the buffer of the *in vivo* system can help improve metabolite production.

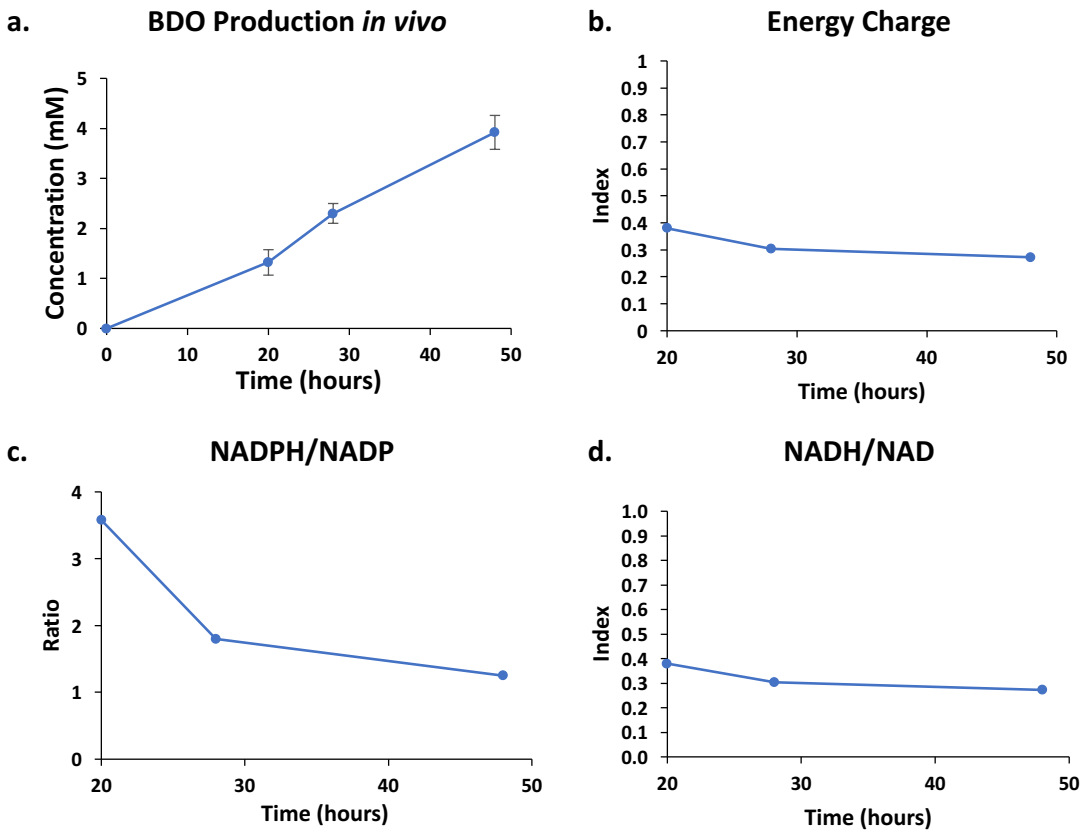

Figure S8: Characteristics of S138 *in vivo*: a. BDO production over time b. pH over time c. Energy charge over time, d. NADPH/NADP and e. NADH/NAD. For c, d, and e: blue—negative control, orange—S138 with the BDO pathway (Data are collected with Construct 4 shown in **Table S1**)

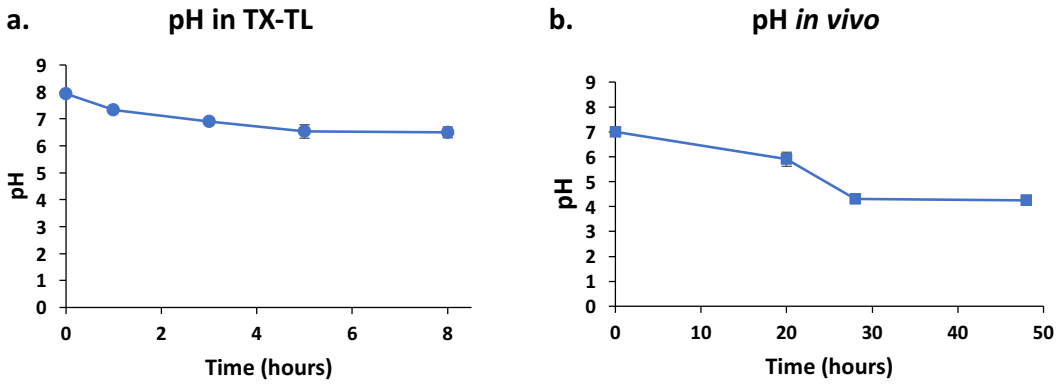

Figure S9: pH comparison between TX-TL and in vivo: a. pH measured over time of TX-TL samples b. pH measured over time of *in vivo* samples

Reference:

1. Fraser, M. E.; James, M. N. G.; Bridger, W. A.; Wolodko, W. T., A detailed structural description of Escherichia coli succinyl-CoA synthetase. *Journal of Molecular Biology* **1999,** *288* (3), 501.
2. Jewett, M. C.; Calhoun, K. A.; Voloshin, A.; Wuu, J. J.; Swartz, J. R., An integrated cell-free metabolic platform for protein production and synthetic biology. *Molecular Systems Biology* **2008,** *4* (1), n/a-n/a.
3. Chen, Y.-J.; Liu, P.; Nielsen, A. A. K.; Brophy, J. A. N.; Clancy, K.; Peterson, T.; Voigt, C. A., Characterization of 582 natural and synthetic terminators and quantification of their design constraints. *Nat Meth* **2013,** *10* (7), 659-664.
4. Yim, H.; Haselbeck, R.; Niu, W.; Pujol-Baxley, C.; Burgard, A.; Boldt, J.; Khandurina, J.; Trawick, J. D.; Osterhout, R. E.; Stephen, R.; Estadilla, J.; Teisan, S.; Schreyer, H. B.; Andrae, S.; Yang, T. H.; Lee, S. Y.; Burk, M. J.; Van Dien, S., Metabolic engineering of Escherichia coli for direct production of 1,4-butanediol. *Nat Chem Biol* **2011,** *7* (7), 445-452.
5. Wishart, D. S.; Knox, C.; Guo, A. C.; Shrivastava, S.; Hassanali, M.; Stothard, P.; Chang, Z.; Woolsey, J., DrugBank: a comprehensive resource for in silico drug discovery and exploration. *Nucleic Acids Research* **2006,** *34* (Database issue), D668-D672.